Geomorphology 413 (2022) 108328

Contents lists available at ScienceDirect

Geomorphology

journal homepage: www.journals.elsevier.com/geomorphology

Eastern Lomonosov Ridge: Constraints for a variable ice mass thickness during former glaciations

Ursula Schlager [a,b,*], Wilfried Jokat [a,b], Estella Weigelt [a], Andrea Catalina Gebhardt [a]

[a] Alfred Wegener Institute Helmholtz Centre for Polar and Marine Research, Am Alten Hafen 26, Bremerhaven 27568, Germany
[b] University of Bremen, Department of Geosciences, Klagenfurter Strasse 4, 28359 Bremen, Germany

ARTICLE INFO

Keywords:
Streamlined glacial lineations
Lomonosov Ridge
Arctic Ocean
Recessional moraines
Pockmarks

ABSTRACT

Here we present dense acoustic and swath bathymetry data sets as well as geological age constraints that allow a new view on past glacial processes at the Siberian termination of Lomonosov Ridge in the Arctic Ocean between 81° and 84° 20′ N. Here, the seabed is marked by three sets of streamlined glacial lineations observed at present water depths of ~760 m to 1250 m. The shallower streamlined glacial lineations were likely formed during MIS 6 and the deeper ones during MIS 12. Other observations include recessional moraines and pockmarks on a flattened ridge crest. In the subsurface, an acoustically transparent unit above well stratified strata is interpreted as subglacial diamicton overlying pre-glacial sediments at an erosional contact. Furthermore, the diamicton is interpreted to have been deposited as lenses in glacially-eroded proximal settings. In contrast, some parts of the seafloor and subsurface show no glacial overprint in water depths as shallow as 819 m. To explain these findings, we propose that the Siberian termination of Lomonosov Ridge was covered by an ice mass of spatial and temporal variable thickness between ~780 to ~1250 m, that was likely composed of sea ice and thick icebergs calved from ice shelves.

1. Introduction

The Arctic Ocean is surrounded by continental shelves broken only by a narrow deep gateway to the Atlantic - the Fram Strait. The continental shelf of the Siberian sector is particularly wide (~700–900 km). Glacial landforms are well known from the seafloor on the shelves and in deeper water of the central Arctic Ocean (e.g., to ~1200 m at the Arlis Plateau) (Polyak et al., 2001; Niessen et al., 2013; Jakobsson et al., 2016; Jakobsson, 2016). Based on a range of evidence, it is known that glacial periods of the past would have seen the Arctic Ocean covered by thick sea ice and/or ice shelves fed by onshore ice catchment areas (Stein et al., 2017). In this context, it is no surprise that the relatively shallow (in places <1000 m deep (Jakobsson et al., 2020)) submarine Lomonosov Ridge hosts numerous glacial landforms (Jakobsson, 1999; Polyak et al., 2001; Kristoffersen et al., 2004; Jakobsson et al., 2008, 2010, 2016).

The ridge is a continental sliver that has undergone continuous subsidence since its breakup from the Barents-Kara-Sea at about 56 Ma (Karasik, 1968; Vogt et al., 1979; Jokat et al., 1995). Its crest is only 60 to 200 km wide but ~1700 km long and at present lies several kilometers above the adjacent deep-sea plains (Jakobsson et al., 2020). It separates the Arctic Ocean into the Eurasia and Amerasia basins.

At the seafloor, the ridge is draped by deposits that are dominated by hemipelagic sediments (Moran et al., 2006) interbedded with ice rafted debris (Stein et al., 2015). Evidence for erosion by moving ice is encountered in water depths down to 1000 m. The ridge crest is bevelled and sculpted by mega-scale glacial lineations (MSGL) and ice scours (Jakobsson, 1999; Polyak et al., 2001; Kristoffersen et al., 2004; Jakobsson et al., 2008, 2010, 2016). At the Siberian termination of Lomonosov Ridge between 81° and 81° 30′ N, two sets of streamlined landforms are reported in even deeper water, to depths of 1280 m (Jakobsson et al., 2016).

Numerous studies propose different explanations for these and other deep-water glacial landforms in the central Arctic Ocean. Kristoffersen et al. (2004) suggest that an armada of icebergs eroded the seabed down to ~980 m water depth in an area between 85° and 87°30′ N on the Siberian side of the ridge. In contrast, Jakobsson et al. (2008) suggest that the same erosion, albeit only the part in present-day water depths of 850 m to 980 m, formed beneath a thick ice shelf that extended across the Lomonosov Ridge from the Barents and Kara seas. In both publications it is suggested that these erosions were possibly created during Marine Isotope Stage (MIS) 6. Mercer (1970) even suggested that an ice

* Corresponding author.
E-mail address: uschlage@awi.de (U. Schlager).

https://doi.org/10.1016/j.geomorph.2022.108328
Received 24 February 2022; Received in revised form 26 May 2022; Accepted 26 May 2022
Available online 30 May 2022

Table 1
Streamers and recording settings used to acquire the data of this study. Whilst operating in close sea-ice conditions, a short streamer was used in both 2018 and 2014. In areas with little or no sea ice, a 3000 m streamer was used instead. In 2018, this 3000 m streamer was composed out of a 2400 m streamer (192 channels and group interval of 12.5 m) and an attached 600 m streamer (96 channels and group interval of 6.25 m).

	2014	2014	2018	2018 (composite streamer)
Streamer length	300 m	3000 m	600 m	2400 m + 600 m = 3000 m
# of channels/group interval	48/ 6.25 m	240/ 12.50 m	96/ 6.25 m	192 + 96 = 288/12.50 m & 6.25 m respectively
Shot point interval	15 s	15 s	~15 s	~10 s
Shot point spacing	~40 m	~40 m	37.5 m	25 m
Recording length	12 s	12 s	14 s	9.5 s
Sample rate	2 ms	1 ms	2 ms	2 ms
Total length of recorded seismic data	287 km	2058 km	788 km	590 km

shelf once covered the entire Arctic Ocean. Gasson et al. (2018) published a modelling study that showed the formation and persistence of such a kilometer-thick pan-Arctic Ice Shelf to be a theoretical possibility under climatic forcing conditions appropriate to MIS 6. Geibert et al. (2021) provided new support for the idea of a pan-Arctic Ice Shelf in the form of two gaps in the ^{230}Th stratigraphy of the Arctic Ocean at ~70–62 ka and ~150–131 ka, i.e., during MIS 4 and 6, respectively. The interpretations were, however, swiftly challenged by Spielhagen et al. (2022) who stated that the low ^{230}Th concentration was caused by high sediment accumulation due to iceberg-rafted terrigenous debris and/or reduced scavenging.

In this contribution, we present an extensive bathymetric data set together with subbottom profiler and multichannel seismic reflection data over the Siberian termination of the Lomonosov Ridge at 81°–84° 20′ N. We describe the distribution of evidence for seafloor erosion by ice and comment on its meaning for the contentious idea of a former kilometer-thick pan-Arctic ice shelf.

2. Methods and data

The swath bathymetry, sediment echosounder and multichannel seismic (MCS) reflection data presented in this study were collected with *RV Polarstern* in September 2014 and 2018. In total, 46,600 km^2 (~17,600 km^2 in 2018; ~29,000 km^2 in 2014) of swath bathymetry profiles were acquired with the ATLAS Hydrographic Hydrosweep DS3 multibeam echo sounder, which is permanently mounted on *RV Polarstern* (Stein, 2015, 2019). In 2014 the swath width was set to 4–5 times water depth. In 2018 a fixed opening angle of 130° was used, resulting in a swath width of 4.3 times water depth. Sound velocity profile casts were collected for water velocity corrections. The data were processed with CARIS HIPS & SIPS software. They were corrected for reflection errors, cleaned of coarse depth errors and gridded with a cell size of 30 × 30 m. A subset of our study area was previously investigated by Jakobsson et al. (2016) and Pérez et al. (2020).

Sediment echosounder data were obtained with a PARASOUND DS III-P70 system mounted on the hull of *RV Polarstern*. For a secondary low frequency of 4 kHz, primary frequencies were set to 18 and 22 kHz in 2018 and 20 and 24 kHz in 2014. Pulse length was 1 ms in 2018 and 0.5 ms in 2014. Secondary low frequency data were recorded in ASD and PS3 format, converted to standard SEGY format and, finally, imported into IHS Kingdom Interpretations software for further visualization and interpretation.

Seismic reflection data were also acquired in 2014 and 2018. Table 1 summarizes the acquisition setups in the two seasons, which differed in response to contrasting sea ice conditions.

The seismic data were processed according to a standard procedure, with a CDP spacing of 25 m, band pass filtering, velocity analysis, spherical divergence and normal moveout correction, and stacking as well as post-stack time migration. A seismic velocity of 1.5 km/s was assumed for calculation of thicknesses within the uppermost ~0.2 s two-way travel-time (TWT) of sediment.

3. Results

Our study area encompasses the Lomonosov Ridge between ~81°–84° 20′ N and 140°–150° E. To aid description, we refer below to its southern and northern parts, either side of 82°N. North of 82°N, the minimum water depth is ~867 m, but most of the ridge crest lies deeper than 1000 m (Fig. 1). South of 82° N, the crest bifurcates to enclose a small intervening basin. Both the western and eastern branches exhibit a flattened ridge top in water depths shallower than 900 m. This southern area is further subdivided into areas I, II and III (Fig. 1). Areas I and II are both shallower than 800 m, reaching a minimum water depth of ~719 m and lie on the eastern branch of the bifurcated ridge. Area III is shallower than 900 m, reaches a minimum water depth of ~819 m and is located on the western branch. The intervening basin plunges gently northwards from ca. 900 m to 1400 m water depth, and blends smoothly with the crest of the Lomonosov Ridge north of 82° N.

The intervening basin and the crest north of 82° N exhibit a smooth seafloor. Sediment echosounder data show coherent parallel, strong subbottom reflections that mimic the seafloor morphology (Fig. 2). Locally these reflections diverge to enclose acoustically transparent lenses (Fig. 2c). The parallel subbottom reflections overlying the lenses are 6 to 12 ms TWT (~4 to 6 m) thick north of 82° N and 12 to 22 ms TWT (~9 to 17 m; mostly ~20 ms TWT) within the intervening basin south of 82° N. South of 81° 22′ N some of the transparent lenses occur in stacks, i.e., in different layers on top of each other (Fig. 2c).

North of 82° N, the smooth domain hosts two areas with circular depressions, one in 900 m deep water at ~84°16′ N, 148°40′ E (Fig. 3a, b) and the other at ~1150 m at ~83°07′ N, 142°40′ E (Figs. 2b, 3c, d). The depressions at ~900 m water depth are around 300 m wide and up to 6 m deep, the ones at ~1150 m are wider (up to 400 m) and deeper (approximately 20 m). Other areas north of 82° N and shallower than 1150 m show no such depressions.

South of 82° N, the flattened crest of the bifurcated Lomonosov Ridge is characterized by an uneven to rough and irregular seafloor (Fig. 4). Subbottom echosounder profiles typically show an upper unit of coherent reflections that lie parallel to the seafloor morphology. This unit overlies an acoustically transparent unit that often overlies a further layer of parallel reflections which, however, follow an internal morphology. The upper part of this bottommost unit is truncated and incised (Fig. 5a, b). MCS data show that the parallel reflection pattern of this unit continues to greater depths (>50 ms; Fig. 5c) than imaged by the sediment echosounder data.

Also south of 82° N, the seafloor is characterized by parallel streamlined seabed lineations, circular depressions (Figs. 4, 6) and small-scale arcuate ridges (Figs. 4, 5b, c). Three different sets of parallel seabed lineations are identified based on their geographical orientation. Set 1 has a west-northwest orientation (Fig. 6). It is imaged at the northern end of area I in ~780 m water depth, as well as in a small area at ~81°25′ and 140°40′ E at ~760 m (Fig. 4b, blue lines; Fig. 6). Set 2, between 81°08′ and 81°44′ °N, can be traced down to water depths of ~1100 m and is northwest oriented (Fig. 4b, dark blue arrows; Fig. 6). Set 3, between 81°06′ and 81°26′ N, has a north-northwest orientation (Fig. 4b, light blue arrows). It is found down to 1250 m. Set 2 overprints set 3 at ~81° 10′ N and ~142°E between 1000 and 850 m water depth. However, this relationship is reversed at ~81° 16′ N and ~141° 15′ E in less than 800 m deep water (Fig. 4b, c). The lineations, with their relief of up to 15 m (set 1: 2–8 m; set 2: 10–15 m; set 3: 10–15 m) and length of up to 11 km (set 1: ≤5 km; set 2: ≤11 km; set3: ≤7 km), are spaced between 100 and 500 m apart (set 1: 100–300 m; set 2: 300–500 m; set 3: 400 m). Sediment echosounder data show that the parallel coherent

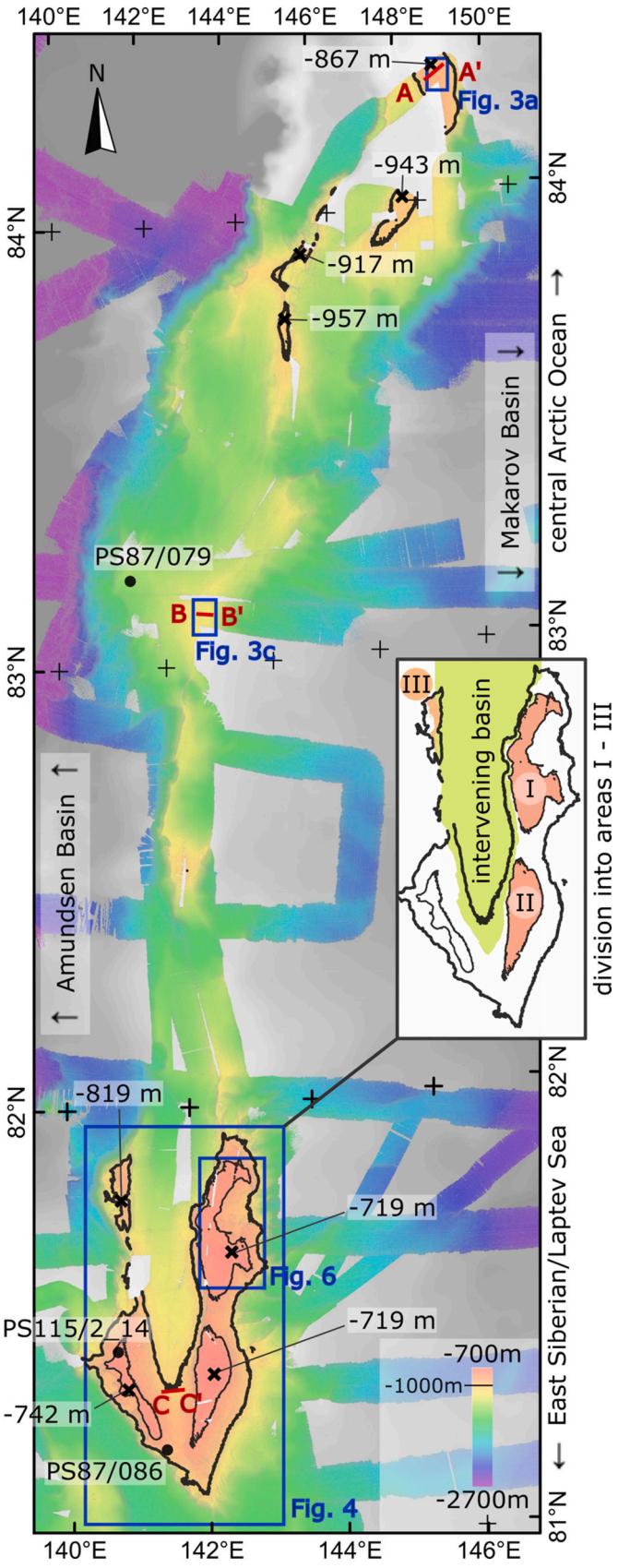

(caption on next column)

Fig. 1. Overview map showing bathymetry data in the study area. The colour bar shows water depth in m. The thick and thin black lines are contour lines along 1000 m and 800 m water depth, respectively; the black crosses mark local peaks shallower than 1000 m with depth values given; black dots show the locations of sediment cores used to date ice-shelf groundings. Sediment echosounder profiles A–A′, B–B′ and C–C′ (red lines) are shown in Fig. 2. The inset figure shows the division of the southern part into areas I, II and III (red) and the intervening basin region (green), marked with its border at 900 m water depth. (For interpretation of the references to colour in this figure legend, the reader is referred to the web version of this article.)

reflections of the uppermost subsurface unit mimic the seafloor morphology of the lineated seafloor. This upper unit is of variable thickness, with ~6–10 ms TWT (~4.5–7.5 m) below set 1 and 12 to 20 ms TWT (~9 and 15 m) below sets 2 and 3. An additional area of glacial overprinting lies at ~83°14′ N and 156°45′ E, away from the Lomonosov Ridge, in water shallower than 800 m (Fig. A.1).

In contrast, other parts of Lomonosov Ridge south of 82° N show no lineations. These include the intervening basin, most parts of areas I and II (Fig. 4) and all of area III (Figs. 4, 7), although all three areas are shallower than 1000 m. Areas I and II are instead characterized by scattered circular depressions and a complex pattern of small ridges (Figs. 4, 6). The circular depressions are up to 700 m in diameter and ≤20 m deep. The small arcuate ridges rise to 3 m above the surrounding seafloor and are aligned with their convex edges towards the north-west.

4. Interpretation and discussion

The Lomonosov Ridge shows a variety of landforms in our research area. We suggest that the parallel seabed lineations, circular depressions and small submarine ridges south of 82° N on the bifurcated ridge crest (Fig. 4) can all be explained by the former presence of grounded ice.

Parallel seabed lineations indicate the action of grounded ice streams (e.g., Boulton, 1976; Clark, 1993). As it moves, grounded ice scours the seabed to create streamlined patterns of parallel ridges and grooves known as streamlined glacial lineations (SGL) (e.g., Clark, 1993; Tulaczyk et al., 2001). We found three different sets of SGL, two of which (sets 2 and 3) had been identified and interpreted as SGL previously (Jakobsson et al., 2016). Set 1 is distinguishable on the basis of its slightly different trend, and is identifiable for the first time here because of the wider coverage of our bathymetric data set (Figs. 4, 6).

The contrasting geographical orientations of these sets indicate three different orientations of ice flow. Based on the strikes of SGL sets 2 and 3, we suggest an ice flow direction from southeast to northwest, i.e., from the Makarov Basin towards the Amundsen Basin (Fig. 4). This ice flow direction conforms with earlier interpretations of Jakobsson et al. (2016) and Jakobsson et al. (2016) for the same region. These SGL do neither appear in the intervening basin nor in area III which is between 900 m and 819 m water depth (Figs. 4, 7). Interestingly, the orientation of all three sets of SGL indicates that the ice masses must have passed this uneroded area III. This would only have been possible if the thickness of the ice reduced significantly as it flowed across the Lomonosov Ridge on its way from the Makarov Basin to the Amundsen Basin or alternatively if its flow stagnated before reaching area III. For set 1 the situation is more complicated. Whilst the orientation of set 1 suggests that the ice responsible for its formation passed over area III, its confinement to water depths of ~760 to 780 m, which is shallower than the seafloor in area III, leaves open the possibility that flowing ice was present, but not grounded there.

Set 2 overprints those of set 3 at ~81°10′ N and 142°0′ E, in water depths between 1000 and 850 m while at ~81°16′ N and 141°15′ E set 3 overprints set 2 (Fig. 4b, c). In the absence of any age constraints estimating the relative ages of the sets are a difficult task. Sediment echosounder data from all of the SGL sets reveal an overlying unit with parallel reflectors that mimic the seafloor topography. The thickness of this unit does not differ significantly between SGL sets 2 and 3 (12–20

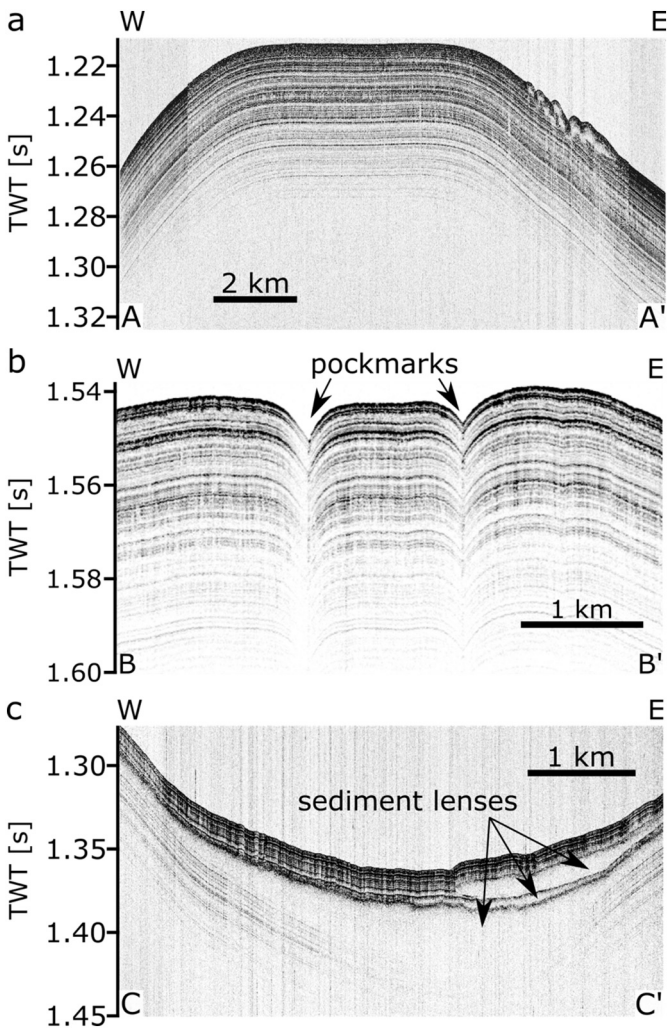

Fig. 2. Sediment echosounder data examples showing coherent parallel reflections of the bathymetrically smooth and gently dipping domain. (a) Profile along A–A′ showing coherent parallel reflections north of 82° N and above 1000 m water depth (~1.33 ms TWT); (b) profile along B–B′ showing coherent parallel reflections interrupted by pockmarks in an area north of 82° N; (c) profile along C–C′ showing coherent parallel reflections with stacked sediment lenses south of 82° N. For profile locations see Fig. 1.

ms TWT; ~9–15 m). Pérez et al. (2020) observed this unit in a subset of our study area (Fig. 4). They report thicknesses of the parallel reflector unit mainly between 10 and 20 ms TWT (7.5–15 m) below both, set 2 and set 3. This suggests that sets 2 and 3 were created around the same time.

SGL of set 1 show no cross-cutting relationship with either of the other sets (Fig. 4b, blue lines). However, assuming constant sedimentation rates, its thinner overlying drape (6–10 ms TWT; ~4.5–7.5 m) suggests that set 1 is likely to be younger than the other sets.

Several sediment cores were taken within the study area during *RV Polarstern* expedition in 2014 and 2018 that help further constrain the formation time of the SGLs. Subbottom profiler data across coring sites show that all these cores (PS87/079, PS87/086 and PS115/2_14) penetrated undisturbed acoustically stratified sediments (Figs. 1, 8a–c). A preliminary age model was proposed for the cores (Stein, 2015; Stein et al., 2016; Stein, 2019), suggesting that the upper ~4.5 m of material in each of them had been deposited during the time interval from MIS 5 to MIS 1, i.e., during the last 130 kyr (Fig. 8d). This implies a mean linear sedimentation rate of ~35 m/Myr. Set 1 SGL, with their minimum drape of 6 ms TWT of sediment (~4.5 m) may thus date to at least ~130 ka (during MIS 6), assuming a constant rate of sedimentation. Under the same assumption, the thicker sediment drapes of sets 2 and 3 (up to 20 ms TWT (~15 m)) date their formation to ~430 ka (MIS 12). This estimate is significantly older (by 290 kyr) than the MIS-6 date (~140 ka) suggested by Jakobsson et al. (2016).

The circular depressions north and south of 82° N are interpreted as pockmarks. Pockmarks are known to result from the vertical flow of fluid or gas from deeper sediment layers to the seafloor (Hustoft et al., 2009). Pore water chemistry tests on a sediment core from Lomonosov Ridge revealed indicators for potential past gas generation but no signs of the presence of present-day free intraformation gas or free gas (Miller et al., 2017). The present-day absence of present-day free intraformation gas and free gas in the subbottom is consistent with our observation in sediment echosounder and MCS data and previous observations of Schlager et al. (2021) in the same study area.

The pockmarks north of 82° N at ~84°16′ N, 148°40′ E and ~83°07′ N, 142°40′ E (Fig. 3) have similar geometries. Although the pockmarks at ~84°16′ N, 148°40′ E are situated close to SGL, chirp sonar subbottom data show no obvious correlation between them (Jakobsson et al., 2016). Unfortunately, the deeper strata below the pockmark fields were not directly imaged with MCS data. However, MCS profile 20,140,280 crossing close to the pockmark field at ~83°11′ N may support an interpretation of differential compaction leading to fluid escape as the cause of both pockmark fields north of 82° N.

The pockmarks south of 82° N in the areas I and II are larger (700 m vs. 400 m) than those north of 82° N. They also have a different topographic expression (Fig. 2b vs. 5a) and are more sparsely distributed (Fig. 3 vs. 6). Furthermore, they are located on the flattened crest of Lomonosov Ridge, in the midst of submarine glacial landforms (Fig. 4). Therefore, and in contrast to the pockmarks north of 82° N, we suggest that their formation might be related to the change from glacial to interglacial times, or more precisely, to the transition from being covered with grounded ice to open water conditions: During glacial times, basal meltwater of grounded ice saturated the underlying sediments with fresh water (Ravier and Buoncristiani, 2018) and in the subsequent interglacial, the grounded ice retreated, the fresh water supply stopped and was replaced by saline water with temperatures below freezing point at the sediment-water interface. The fresh water in the saturated sediment consequently froze and, by virtue of its lower density, rafted away as ice, carrying small amounts of sediments off the seafloor (Paull et al., 1999). In this way, an excavation successively develops (Paull et al., 1999). We suggest that such a scenario could have created the pockmarks south of 82° N, not least because they are amidst submarine glacial landforms.

The small submarine arcuate ridges in area I were first described by Jakobsson et al. (2016). Together with the sediment echosounder and MCS data from this study, we interprete them as recessional moraines (Fig. 5b, c). Their arcuate shapes indicate a northwesterly ice flow direction during a period of stepwise ice sheet retreat towards the southwest (Dove et al., 2014).

Sediment echosounder data show that the crest of Lomonosov Ridge south of 82° N hosts a layer that is acoustically transparent (Figs. 5a, b, 8b, c). This layer is also reported by Pérez et al. (2020). The layer has a rough upper surface whose topography is mimicked by the overlying and uppermost unit of mostly coherent parallel reflections. This relationship results in the rough morphology at the seafloor, which hosts SGLs, pockmarks and recessional moraines - all features whose formation we have previously associated with glacial processes. Moving ice sheets form subglacial diamicton by deforming soft sediment at their base (Dowdeswell et al., 2007). Diamicton consists of unsorted to poorly sorted sediment. The lack of organized lithological contrasts, such as bedding planes, to act as consistent reflectors of seismic energy means that diamicton tends to be transparent in sediment echosounder images. Therefore, we suggest the acoustically transparent layer consists of subglacial diamicton. After retreat of the ice sheet, hemipelagic sediments draped over the diamicton body. These more organized sediments

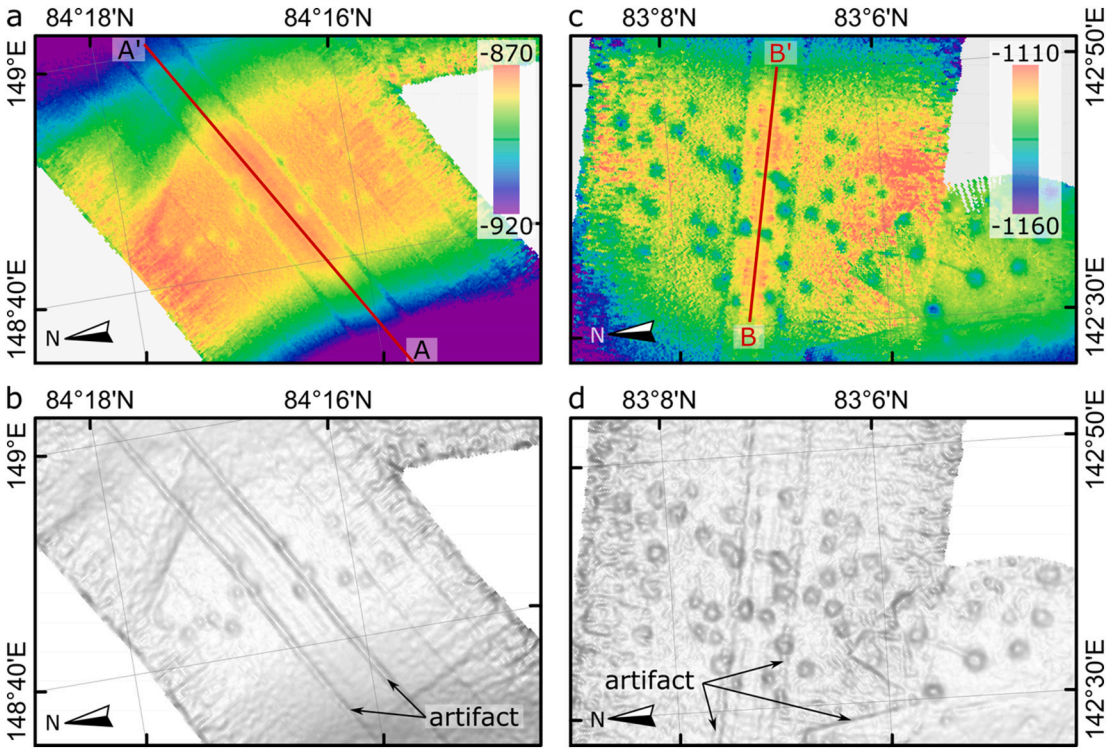

Fig. 3. Pockmarks on Lomonosov Ridge in the bathymetrically smooth and gently dipping domain north of 82° N. (a, c) Bathymetric map showing the pockmarks. Colour bar: water depths in m; (b, d) Pockmarks emphasized using the ArcGIS slope calculation. Sediment echosounder data along profiles A–A′ and B–B′ are shown in Fig. 2. For locations see Fig. 1.

are imaged in sediment echosounder data. Pérez et al. (2020) showed that the acoustically transparent layer extends over the whole crest of Lomonosov Ridge between 81° and 82° N. Consequently, it seems that the whole ridge crest of Lomonosov Ridge between 81° and 82° N is covered with diamicton that itself is buried under hemipelagic sediments 4–17 m (6–22 ms TWT) thick.

In comparison, other parts of our research area, namely the intervening basin and the rigde crest north of 82° N, do not show any signs of glacial erosion at the seafloor or in their deeper stratigraphy. Instead, they contain predominantly undisturbed sediments that are occasionally interbedded with acoustically transparent material. Subbottom echosounder data reveal these lenses to be present at various stratigraphic levels (Fig. 2c), and to be concentrated in the intervening basin, which is flanked by the glacially eroded crests the bifurcated Lomonosov Ridge. Similar to the suggestion of Jakobsson et al. (2008) for the Lomonosov Ridge at 84°–87°30′N, 140°–160° E, we consider the acoustically transparent lenses transported by downslope debris flow of till into the basin from the surrounding ridge crest in periods when it was cleared of glacial debris by grounded ice. Therefore, we assume that the acoustically transparent lenses consist of reworked diamicton from the surrounding ridge crest.

Previous studies from other parts of the Lomonosov Ridge revealed that glaciogenic features are nearly ubiquitous at depths shallower than ~1000 m (Fig. 9). Glacial erosion to this present-day depth during past glacial maxima would require a paleo-ice mass with a ~1 km thickness, considering a 120 m lower sea level during glacial times (Miller et al., 2020) and that 10% a floating ice mass lies above sea level. The question of whether a pan-Arctic ice shelf of such a thickness ever existed cannot be answered definitively from this study, which covers only a small portion of the Arctic Ocean. We can, however, contribute to the question of the thickness of such an ice mass by noting that our study adds (i) more examples of locations along the Lomonosov Ridge in water depths as shallow as 819 m that show no evidence for subglacial erosion, (ii) more examples of locations that do show evidence for subglacial erosion in water as deep as 1250 m, and (iii) evidence for at least two different periods of SGL formation on the crest of the Lomonosov Ridge. Our observations thus support the idea of ice thickness and grounding patterns with considerable spatial and temporal variability.

Considering as before a 120 m lower sea level during glacial times (Miller et al., 2020) and that 90% of floating ice mass is present below sea level, our observations alone suggest ice masses thicknesses that varied between ~1250 m and ~780 m in a relatively small area. We suggest that this variability might indicate the existence of a composite ice mass, for example one composed of multiple thick ice shelf fragments of very large areal extents, detached from the ice sheets on the Arctic continental shelves (Niessen et al., 2013) but surrounded by relatively thin but complete multi-year sea ice. An alternative scenario to explain our observations might involve an ice shelf that is thick next to its grounding line on the continental shelf and considerably thinner further out in the central Arctic Ocean. This hypothesis, however, requires a mechanism for the thinning that is not immediately apparent to us. We favour, hence, our first proposal of a composite ice mass as this hypothesis is able to explain glacially eroded features also on other parts of Lomonosov Ridge outside of our study area.

5. Conclusions

Like the Arctic Ocean's continental margins, the Lomonosov Ridge that crosses its middle shows evidence for having been strongly modified by glaciers and ice streams. In our study, located between ~81°–84° 20′ N and 140°–150° E at the eastern Lomonosov Ridge, we observed numerous submarine landforms from which those south of 82° N are of glacial origin:

- A flattened ridge crest at ~800–719 m water depth: subbottom data here reveal a bottommost layer with well-stratified but truncated and incised sediment. This layer is overlain by a potential diamicton that in turn is draped by hemipelagic sediments.

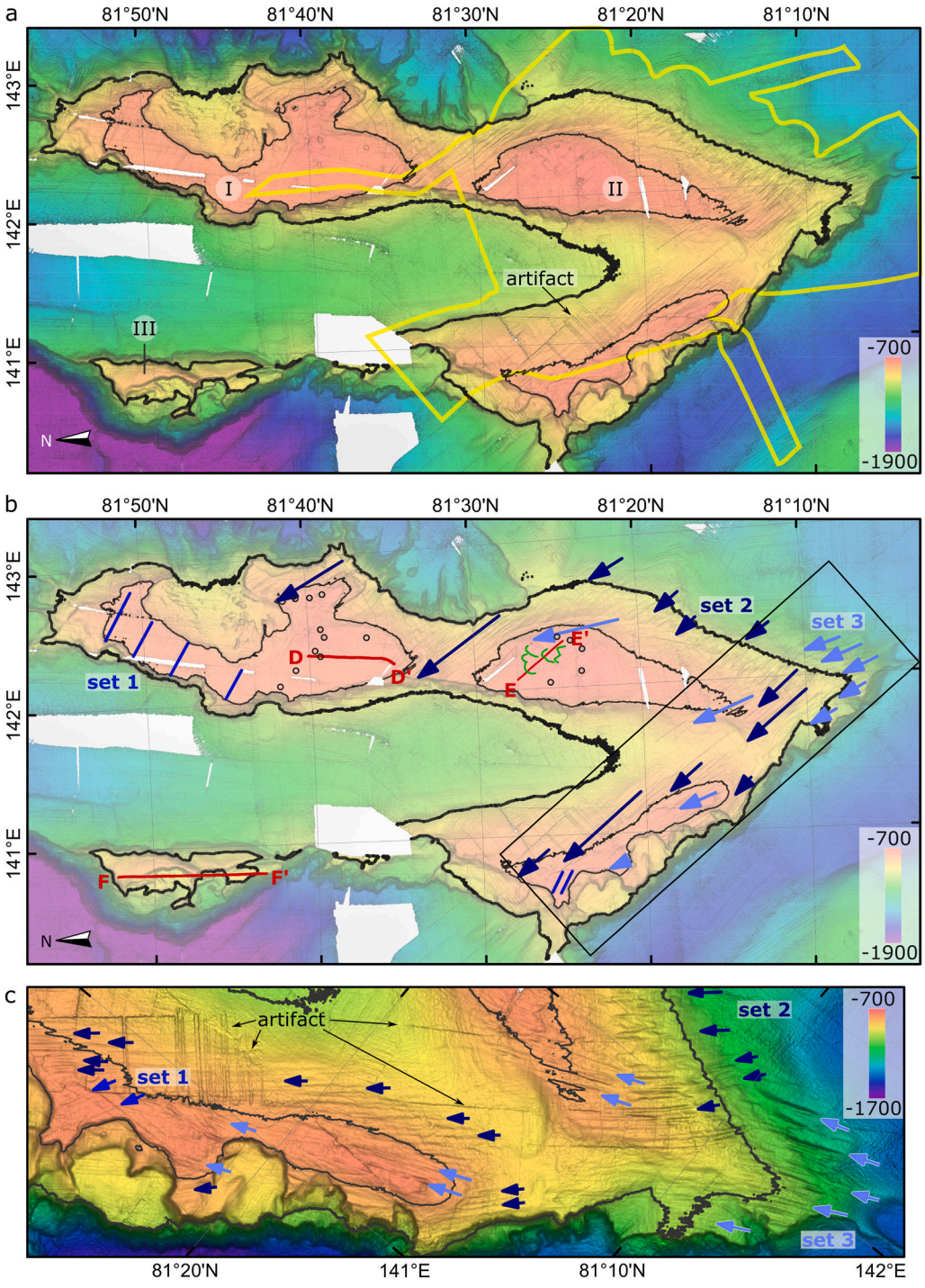

Fig. 4. Lomonosov Ridge between ~81° and 82° N showing the flat ridge crest, SGL, pockmarks and recessional moraines. (a) bathymetric map showing glacial landforms; yellow outlined area: area studied by Jakobsson et al. (2016) and Pérez et al. (2020); (b) the same map as in (a) but with interpreted SGLs of set 1 (blue lines), set 2 (dark blue arrows) and set 3 (light blue arrows) as well as pockmarks (black circles) and recessional moraines (green lines). Sediment echosounder profiles between D–D′ and E–E′ (red lines) are shown in Fig. 5 and between F–F′ is shown in Fig. 7. (c) zoom to area shown in (b), the arrows point to glacial lineations. The colour bar shows water depths in m. The thin and thick black lines mark the 800 m and 1000 m contour line, respectively. (For interpretation of the references to colour in this figure legend, the reader is referred to the web version of this article.)

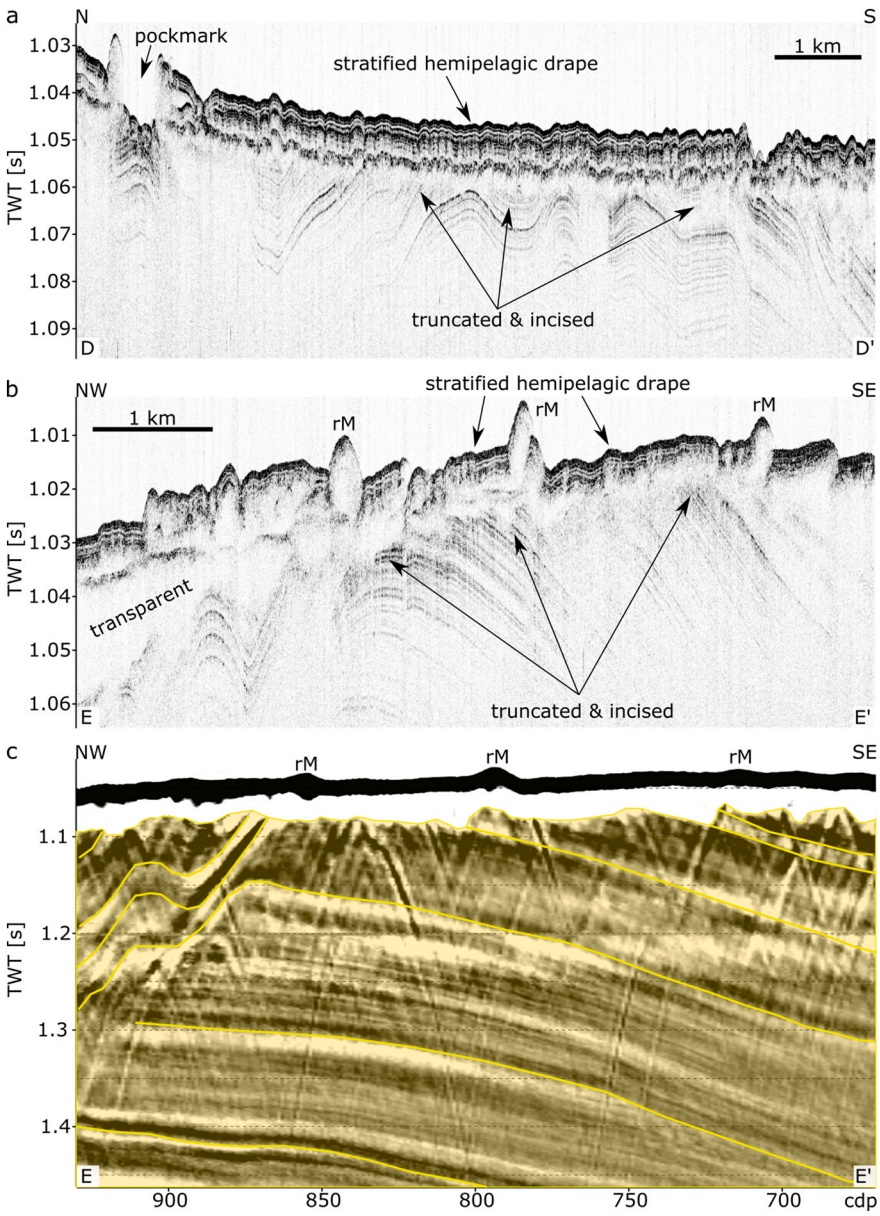

Fig. 5. Sediment echosounder and MCS profiles of Lomonosov Ridge south of 82° N showing typical sub-bottom reflection patterns south of 82° N including reflection patterns of pockmarks and recessional moraines. (a, b) sediment echosounder data along profiles D–D′ and E–E′ showing a bottommost layer of parallel reflections that follow an internal morphology and are truncated and incised at the top, an overlying layer of acoustically transparent reflections with variable thickness and an upper layer with coherent parallel reflections that reflect the seafloor morphology. Automatic Gain Control with a 100 ms time window was applied to better highlight the lower stratigraphy. (c) MCS profile (AWI-20140314) for data shown in (b), showing that the lowest layer visible in (b) with its parallel reflections can be traced to greater depths (yellow area). cdp: common depth point; rM: recessional moraine. For locations of the profiles see Fig. 4.

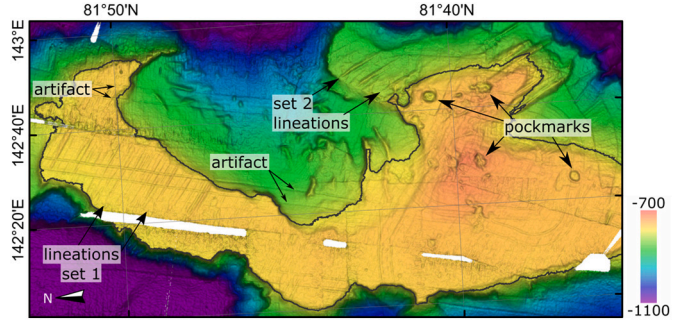

Fig. 6. Area of Lomonosov Ridge above 800 m water depths (south of 82° N) showing Pockmarks and SGL of sets 1 and 2. black contour line: 800 m water depth; colour bar: water depths in m. For location see Fig. 1.

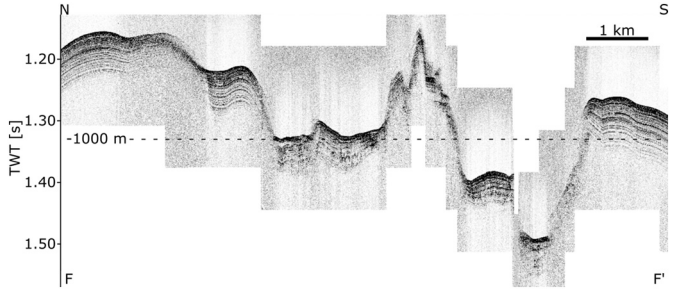

Fig. 7. Sediment echosounder data along the glacially uneroded area on Lomonosov Ridge at ~81°50′ N and 140°50′ E showing well stratified sub-bottom reflections above 1000 m water depth (dashed line). Automatic Gain control with a time window of 250 ms was applied on data. For location of the profile see Fig. 4.

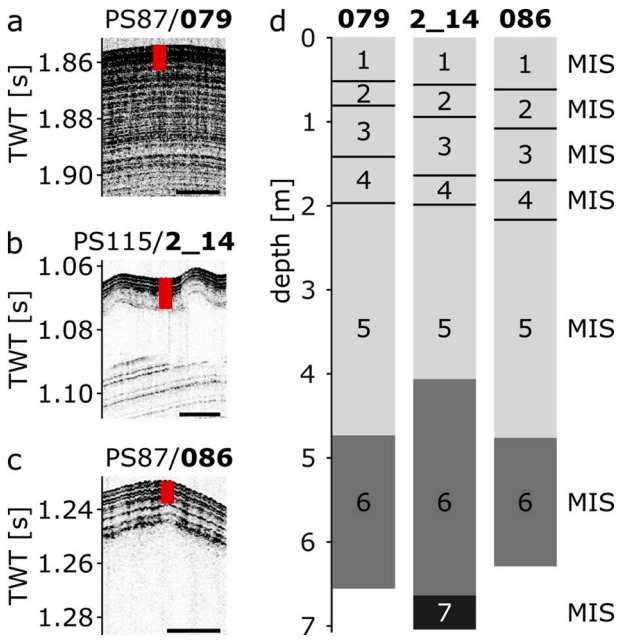

Fig. 8. Sediment echosounder profiles around core positions and preliminary age estimates. (a–c) Subbottom reflection pattern around and below the sediment cores showing coherent parallel reflections. Red rectangles: core position and time-converted core length; thick horizontal line: 200 m scale bar. (d) Dated sediment cores using the preliminary proposed age model (Stein, 2015, 2019). Core age profiles modified after (Stein, 2015) and (Stein, 2019). For location see Fig. 1. (For interpretation of the references to colour in this figure legend, the reader is referred to the web version of this article.)

- o Recessional moraines that indicate a stepwise retreat of grounded ice.
- o Pockmarks that might be related to the former presence of grounded ice as explained in the text.
- o Three sets of SGL with consistent contrasting orientations; west-northwest, northwest and north-northwest. The SGL are present to water depths as deep as ~1250 m on the Makarov Basin side of Lomonosov Ridge and as shallow as to 760 m on the ridge crest. The SGL were likely created during two periods, in MIS 6 and MIS 12.

As well as these glacially-affected parts of the ridge, there is also an area south of 82° N rising up to 819 m water depth that appears unaffected by glacial erosion and therefore points at an ice flow direction from the Makarov Basin to the Amundsen Basin.

The Lomonosov Ridge north of 82° N displays a smooth seafloor with well-stratified layers in the subsurface except in two local areas of pockmarks that might be created by differential compaction due to fluid escape. This region rises locally to seafloor depths shallower than 1000 m water depth, but nonetheless reveals no signs of glacial erosion.

Our data support the hypothesis of an ice mass with a large enough area to impart regionally-coherent SGL patterns (as opposed to the more chaotic characteristics of iceberg ploughmarks) but with a variable thickness ranging between 1250 m and 780 m. We favour an interpretation that such an ice mass was likely a composite ice mass, i.e., one composed of sea ice that enclosed much thicker fragments calved from multiple ice shelves situated around the margins of the Arctic Ocean. In contrast to the hypothesis of a kilometer-thick pan-Arctic ice shelf, the hypothesis of a composite ice mass whose thickness exceeds a kilometer in some areas explains both glacially eroded and non-eroded areas on the Lomonosov Ridge, that are both observed on the ridge in water depths shallower than 1000 m.

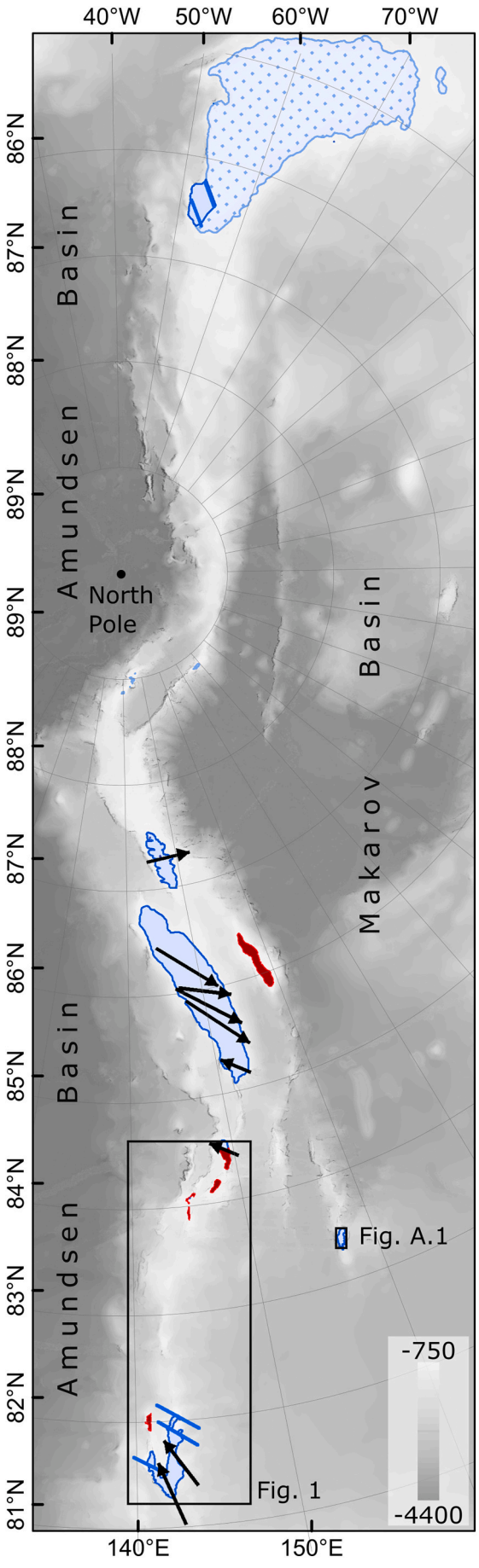

(caption on next page)

Fig. 9. Reported glacial landforms on the whole Lomonosov Ridge from this and previous studies including this one. All coloured areas (red and blue) mark water depths shallower than 1000 m: blue filled and outlined areas: ice eroded areas; black arrows: suggested ice flow directions for reported SGL; blue lines: orientations of reported SGL (without suggested ice flow direction by the authors); red filled areas: areas without evidence for glacial erosion; blue filled and dotted area: a shallow area on Lomonosov Ridge for which no information about potential ice erosion is available yet. Source: (Polyak et al., 2001; Kristoffersen et al., 2004; Jakobsson et al., 2008; Jakobsson et al., 2016 and this study); gray colour bar: water depths in m. Bathymetry taken from IBCAO v4 (Jakobsson et al., 2020). (For interpretation of the references to colour in this figure legend, the reader is referred to the web version of this article.)

Data availability

The bathymetric, sediment echosounder and seismic data sets acquired in 2014 are archived under at https://doi.pangaea.de/10.1594/PANGAEA.857857, https://doi.pangaea.de/10.1594/PANGAEA.839763 and https://doi.pangaea.de/10.1594/PANGAEA.919774, respectively. The bathymetric and sediment echosounder data sets acquired in 2018 are archived under https://doi.pangaea.de/10.1594/PANGAEA.916120 and https://doi.org/10.1594/PANGAEA.916109, respectively. The seismic data gained in 2018 are uploaded to PANGAEA-database and still under moratorium but are available on enquiry.

Declaration of competing interest

The authors declare that they have no known competing financial interests or personal relationships that could have appeared to influence the work reported in this paper.

Acknowledgments

We thank the captain and crew of *RV Polarstern* Expedition PS87 and PS115/2 as well as all members of the geophysical and hydroacoustic teams on board for their support in getting geophysical data. We further thank our colleagues from AWI- bathymetry group Laura Jensen and Simon Dreutter for providing us with bathymetry grid data as well as Hanno Keil (University of Bremen) for the ps32sgy tool enabling us to convert PS3 format to standard SGY format. Many thanks to G. Eagles for helpful comments as well as J. E. Arndt and K. Repenning for friendly and helpful software introductions. We further thank our anonymous reviewers for constructive suggestions for the manuscript that led to essential improvements. Finally, we would like to thank Emerson E&P Software, Emerson Automation Solutions, for providing licenses for the seismic software Paradigm in the scope of the Emerson Academic Program and IHS Markit for providing an academic license of IHS Kingdom for data interpretation. This research did not receive any specific grant from funding agencies in the public, commercial, or not-for-profit sectors.

Appendix A

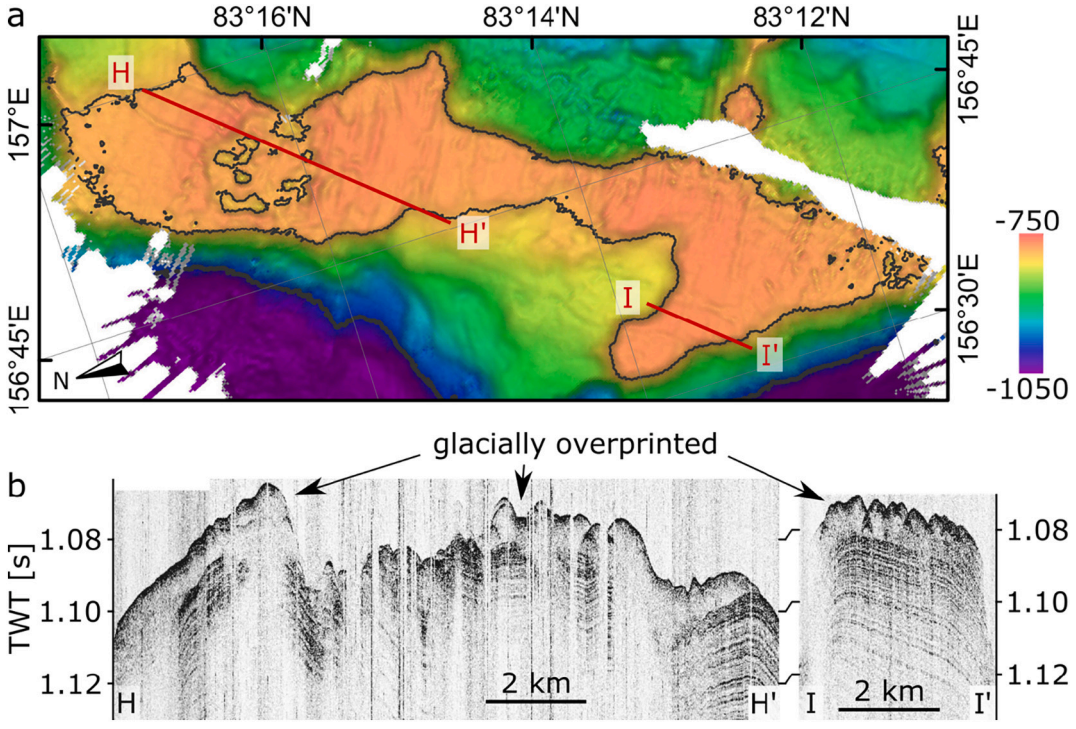

Fig. A.1. Glacially overprinted area off the Lomonosov Ridge. (a) Bathymetric map showing the glacially overprinted area. Black contour line: 800 m water depth; colour bar: water depths in m. (b) Sediment echosounder data showing a glacially overprinted subbottom. For location see Fig. 9.

References

Boulton, G.S., 1976. The origin of glacially fluted surfaces-observations and theory. J. Glaciol. 17 (76), 287–309. https://doi.org/10.3189/S0022143000013605.

Clark, C.D., 1993. Mega-scale glacial lineations and cross-cutting ice-flow landforms. Earth Surf. Process. Landf. 18 (1), 1–29. https://doi.org/10.1002/esp.3290180102.

Dove, D., Polyak, L., Coakley, B., 2014. Widespread, multi-source glacial erosion on the Chukchi margin, Arctic Ocean. Quat. Sci. Rev. 92, 112–122. https://doi.org/10.1016/j.quascirev.2013.07.016.

Dowdeswell, J., Ottesen, D., Rise, L., Craig, J., 2007. Identification and preservation of landforms diagnostic of past ice-sheet activity on continental shelves from three-dimensional seismic evidence. Geology 35, 359–362. https://doi.org/10.1130/G23200A.1.

Gasson, E.G.W., DeConto, R.M., Pollard, D., Clark, C.D., 2018. Numerical simulations of a kilometre-thick Arctic ice shelf consistent with ice grounding observations. Nat. Commun. 9 (1), 1510. https://doi.org/10.1038/s41467-018-03707-w.

Geibert, W., Matthiessen, J., Stimac, I., Wollenburg, J., Stein, R., 2021. Glacial episodes of a freshwater Arctic Ocean covered by a thick ice shelf. Nature 590 (7844), 97–102. https://doi.org/10.1038/s41586-021-03186-y.

Hustoft, S., Bünz, S., Mienert, J., Chand, S., 2009. Gas hydrate reservoir and active methane-venting province in sediments on <20 Ma young oceanic crust in the Fram Strait, offshore NW-Svalbard. Earth Planet. Sci. Lett. 284 (1), 12–24. https://doi.org/10.1016/j.epsl.2009.03.038.

Jakobsson, M., 1999. First high-resolution chirp sonar profiles from the Central Arctic Ocean reveal erosion of Lomonosov Ridge sediments. Mar. Geol. 158 (1–4), 111–123. https://doi.org/10.1016/S0025-3227(98)00186-8.

Jakobsson, M., 2016. Submarine glacial landform distribution in the central Arctic Ocean shelf-slope-basin system. In: Dowdeswell, J.A., Canals, M., Jakobsson, M., Todd, B.J., Dowdeswell, E.K., Hogan, K.A. (Eds.), Atlas of Submarine Glacial Landforms: Modern, Quaternary and Ancient, Geological Society, London, Memoirs, 46, pp. 469–476. https://doi.org/10.1144/M46.179.

Jakobsson, M., Polyak, L., Edwards, M., Kleman, J., Coakley, B., 2008. Glacial geomorphology of the Central Arctic Ocean: the Chukchi Borderland and the Lomonosov Ridge. Earth Surf. Process. Landf. 33 (4), 526–545. https://doi.org/10.1002/esp.1667.

Jakobsson, M., Nilsson, J., O'Regan, M., Backman, J., Löwemark, L., Dowdeswell, J.A., Mayer, L., Polyak, L., Colleoni, F., Anderson, L.G., Björk, G., Darby, D., Eriksson, B., Hanslik, D., Hell, B., Marcussen, C., Sellén, E., Wallin, T., 2010. An Arctic Ocean ice shelf during MIS 6 constrained by new geophysical and geological data. Quat. Sci. Rev. 29 (25–26), 3505–3517. https://doi.org/10.1016/j.quascirev.2010.03.015.

Jakobsson, M., Nilsson, J., Anderson, L., Backman, J., Björk, G., Cronin, T.M., Kirchner, N., Koshurnikov, A., Mayer, L., Noormets, R., O'Regan, M., Stranne, C., Ananiev, R., Barrientos Macho, N., Cherniykh, D., Coxall, H., Eriksson, B., Flodén, T., Gemery, L., Gustafsson, Ö., Jerram, K., Johansson, C., Khortov, A., Mohammad, R., Semiletov, I., 2016. Evidence for an ice shelf covering the Central Arctic Ocean during the penultimate glaciation. Nat. Commun. 7, 10365. https://doi.org/10.1038/ncomms10365.

Jakobsson, M., Mayer, L.A., Bringensparr, C., Castro, C.F., Mohammad, R., Johnson, P., Ketter, T., Accettella, D., Amblas, D., An, L., Arndt, J.E., Canals, M., Casamor, J.L., Chauché, N., Coakley, B., Danielson, S., Demarte, M., Dickson, M.-L., Dorschel, B., Dowdeswell, J.A., Dreutter, S., Fremand, A.C., Gallant, D., Hall, J.K., Hehemann, L., Hodnesdal, H., Hong, J., Ivaldi, R., Kane, E., Klaucke, I., Krawczyk, D.W., Kristoffersen, Y., Kuipers, B.R., Millan, R., Masetti, G., Morlighem, M., Noormets, R., Prescott, M.M., Rebesco, M., Rignot, E., Semiletov, I., Tate, A.J., Travaglini, P., Velicogna, I., Weatherall, P., Weinrebe, W., Willis, J.K., Wood, M., Zarayskaya, Y., Zhang, T., Zimmermann, M., Zinglersen, K.B., 2020. The international bathymetric chart of the Arctic Ocean version 4.0. Sci. Data 7 (1), 176. https://doi.org/10.1038/s41597-020-0520-9.

Jokat, W., Weigelt, E., Kristoffersen, Y., Rasmussen, T., Schöne, T., 1995. New insights into the evolution of the Lomonosov Ridge and the Eurasian Basin. Geophys. J. Int. 122 (2), 378–392. https://doi.org/10.1111/j.1365-246X.1995.tb00532.x.

Karasik, A.M., 1968. Magnetic anomalies of the Gakkel Ridge and origin of the Eurasia Subbasin of the Arctic Ocean. Geofizicheskie Metody Razvedki Arktike 5, 8–19 (Russian).

Kristoffersen, Y., Coakley, B., Jokat, W., Edwards, M., Brekke, H., Gjengedal, J., 2004. Seabed erosion on the Lomonosov Ridge, Central Arctic Ocean: a tale of deep draft icebergs in the Eurasia Basin and the influence of Atlantic water inflow on iceberg motion? Paleoceanography 19 (3), 3001–3014. https://doi.org/10.1029/2003PA000985. PA3006.

Mercer, J.H., 1970. A former ice sheet in the Arctic Ocean? Palaeogeogr. Palaeoclimatol. Palaeoecol. 8 (1), 19–27. https://doi.org/10.1016/0031-0182(70)90076-3.

Miller, C.M., Dickens, G.R., Jakobsson, M., Johansson, C., Koshurnikov, A., O'Regan, M., Muschitiello, F., Stranne, C., 2017. Pore water geochemistry along continental slopes north of the East Siberian Sea: inference of low methane concentrations. Biogeosciences 14 (12), 2929–2953. https://doi.org/10.5194/bg-14-2929-2017.

Miller, K.G., Browning, J.V., Schmelz, W.J., Kopp, R.E., Mountain, G.S., Wright, J.D., 2020. Cenozoic sea-level and cryospheric evolution from deep-sea geochemical and continental margin records. Sci. Adv. 6 (20), eaaz1346 https://doi.org/10.1126/sciadv.aaz1346.

Moran, K., Backman, J., Brinkhuis, H., Clemens, S.C., Cronin, T., Dickens, G.R., Eynaud, F., Gattacceca, J., Jakobsson, M., Jordan, R.W., Kaminski, M., King, J., Koc, N., Krylov, A., Martinez, N., Matthiessen, J., McInroy, D., Moore, T.C., Onodera, J., O'Regan, M., Pälike, H., Rea, B., Rio, D., Sakamoto, T., Smith, D.C., Stein, R., St John, K., Suto, I., Suzuki, N., Takahashi, K., Watanabe, M., Yamamoto, M., Farrell, J., Frank, M., Kubik, P., Jokat, W., Kristoffersen, Y., 2006. The Cenozoic palaeoenvironment of the Arctic Ocean. Nature 441 (7093), 601–605. https://doi.org/10.1038/nature04800.

Niessen, F., Hong, J.K., Hegewald, A., Matthiessen, J., Stein, R., Kim, H., Kim, S., Jensen, L., Jokat, W., Nam, S.I., Kang, S.H., 2013. Repeated Pleistocene glaciation of the East Siberian Continental margin. Nat. Geosci. 6 (10), 842–846. https://doi.org/10.1038/ngeo1904.

Paull, C.K., Ussler Iii, W., Borowski, W.S., 1999. Freshwater ice rafting: an additional mechanism for the formation of some high-latitude submarine pockmarks. Geo-Mar. Lett. 19 (1–2), 164–168. https://doi.org/10.1007/s003670050104.

Pérez, L.F., Jakobsson, M., Funck, T., Andresen, K.J., Nielsen, T., O'Regan, M., Mørk, F., 2020. Late Quaternary sedimentary processes in the Central Arctic Ocean inferred from geophysical mapping. Geomorphology 369, 107309. https://doi.org/10.1016/j.geomorph.2020.107309.

Polyak, L., Edwards, M.H., Coakley, B.J., Jakobsson, M., 2001. Ice shelves in the Pleistocene Arctic Ocean inferred from glaciogenic deep-sea bedforms. Nature 410 (6827), 453–457. https://doi.org/10.1038/35068536.

Ravier, E., Buoncristiani, J.F., 2018. Chapter 12 - Glaciohydrogeology. In: Menzies, J., van der Meer, J.J.M. (Eds.), Past Glacial Environments, Second edition. Elsevier, pp. 431–466. https://doi.org/10.1016/B978-0-08-100524-8.00013-0st.

Schlager, U., Jokat, W., Weigelt, E., Gebhardt, C., 2021. Submarine landslides along the Siberian termination of the Lomonosov Ridge, Arctic Ocean. Geomorphology 382, 107679. https://doi.org/10.1016/j.geomorph.2021.107679.

Spielhagen, R.F., Scholten, J.C., Bauch, H.A., Eisenhauer, A., 2022. No freshwater-filled glacial Arctic Ocean. Nature 602 (7895), E1–E3. https://doi.org/10.1038/s41586-021-04089-8.

Stein, R., 2015. The Expedition PS87 of the Research Vessel POLARSTERN to the Arctic Ocean in 2014. Alfred Wegener Institute for Polar and Marine Research, Bremerhaven. https://doi.org/10.2312/BzPM_0688_2015.

Stein, R., 2019. The Expedition PS115/2 of the Research Vessel POLARSTERN to the Arctic Ocean in 2018. Alfred Wegener Institute for Polar and Marine Research, Bremerhaven. https://doi.org/10.2312/BzPM_0728_2019.

Stein, R., Jokat, W., Niessen, F., Weigelt, E., 2015. Exploring the long-term Cenozoic Arctic Ocean climate history: a challenge within the International Ocean Discovery Program (IODP). Arktos 1 (1), 3. https://doi.org/10.1007/s41063-015-0012-x.

Stein, R., Fahl, K., Schreck, M., Knorr, G., Niessen, F., Forwick, M., Gebhardt, C., Jensen, L., Kaminski, M., Kopf, A., Matthiessen, J., Jokat, W., Lohmann, G., 2016. Evidence for ice-free summers in the late Miocene Central Arctic Ocean. Nat. Commun. 7 (1), 11148. https://doi.org/10.1038/ncomms11148.

Stein, R., Fahl, K., Gierz, P., Niessen, F., Lohmann, G., 2017. Arctic Ocean sea ice cover during the penultimate glacial and the last interglacial. Nat. Commun. 8 (1), 373. https://doi.org/10.1038/s41467-017-00552-1.

Tulaczyk, S.M., Scherer, R.P., Clark, C.D., 2001. A ploughing model for the origin of weak tills beneath ice streams: a qualitative treatment. Quat. Int. 86 (1), 59–70. https://doi.org/10.1016/S1040-6182(01)00050-7.

Vogt, P.R., Taylor, P.T., Kovacs, L.C., Johnson, G.L., 1979. Detailed aeromagnetic investigation of the Arctic Basin. J. Geophys. Res. Solid Earth 84 (B3), 1071–1089. https://doi.org/10.1029/JB084iB03p01071.